ELSEVIER

Contents lists available at ScienceDirect

Surface & Coatings Technology

journal homepage: www.elsevier.com/locate/surfcoat





Computational tool for analyzing stress in thin films

Eric Chason*, Tong Su, Zhaoxia Rao

School of Engineering, Brown University, Providence, RI 02912, United States

ARTICLE INFO

Keywords: Thin films Residual stress Energetic deposition Computer model

ABSTRACT

A computational model has been developed to analyze calculations of residual stress in thin films determined from in-situ wafer curvature measurements. The model is based on several physical mechanisms that have been proposed to control the stress, including the effect of growth kinetics, grain growth and energetic particle bombardment. From a set of data, the program determines a set of kinetic parameters that can be used to understand the processes controlling stress. These parameters can be used to estimate the stress that will develop under different processing conditions in order to obtain a desired stress state. Several examples are described that illustrate the program's capabilities, including the effects of growth rate, growth temperature and particle energy (via chamber pressure in sputter deposition). Interested researchers may obtain the program and associated documentation to use the program to analyze their own data.

1. Introduction

Residual stress in thin films, i.e., the kind that develops during deposition, impacts their performance and reliability. Since stress is affected by many parameters (growth rate, temperature, microstructural evolution, composition, particle energy for sputter deposition, etc.), it can be modified by the choice of processing conditions. Being able to predict how it depends on the growth parameters would enable it to be efficiently optimized.

Over the past few years, a kinetic model for the evolution of thin film stress under different conditions [1] has been developed. The model is based on physical mechanisms that describe how different kinetic processes that occur during film growth contribute to the evolution of stress in the film. This work describes how this model has been implemented in a computer program that enables the user to analyze wafer curvature measurements of stress. This produces a set of kinetic parameters that can then be used to predict and optimize the film stress.

The program is written as an application using the MATLAB® software. Avenues for obtaining the code and associated documentation are discussed at the end of the manuscript. For users who do not have access to MATLAB, a standalone version is also available.

1.1. Background

There is a large literature documenting the evolution of stress in different materials and by different deposition methods. Descriptions of

prior results can be found in multiple reviews [2–6]. The observed dependence of the stress on processing conditions, materials properties and microstructural evolution are features that must be successfully explained by a model of stress. Some key observations that have emerged from these studies are summarized below.

The work of Koch and Abermann [7] showed that, depending on intrinsic material properties (e.g., melting point) and processing conditions (e.g., deposition rate and temperature) two types of stress evolution scenarios are possible, denoted as type I (low mobility) and type II (high mobility). They found that in low mobility films (type I), the stress is consistently tensile as the thickness increases. Further, when the deposition is paused, the stress does not change. In contrast, for materials with high atomic mobility (type II), the stress becomes tensile during the early stages of growth but then becomes compressive as the thickness increases. When the deposition is paused, the stress relaxes significantly. The type of stress evolution behavior can be modified by changing the growth rate and/or growth temperature, e.g., type I behavior is promoted by raising the growth rate [8] or lowering the growth temperature [5].

The stress evolution is also intimately tied to the evolution of the microstructure. For type II growth, the stress changes from tensile to compressive when the film transitions from isolated nuclei into a continuous film as the thickness increases [9]. Increasing the grain size at the film's surface changes the stress in new layers added to the film [10]. Subsurface grain growth in the existing film can induce additional stress by removing grain boundaries and densifying the film [11].

E-mail address: eric_chason_phd@brown.edu (E. Chason).

^{*} Corresponding author.

The stress can be further modified by the addition of energy to the deposited particles or other species as in sputter deposition [12]. This enables the growth of refractory materials with high density and compressive stress, properties that are difficult to achieve with non-energetic deposition.

1.2. Principle of wafer curvature

Many measurements of stress are obtained using the wafer curvature technique [5,13]. This allows the stress to be measured in real-time by monitoring the curvature it induces in the substrate, typically by optical techniques. Since the model in this work is designed to interpret these types of experiments, it is useful to briefly review the physical principles underlying the technique. Multiple methods have been developed that enable the curvature to be measured while the film is being deposited but these are not discussed here (see ref. [5] for a brief review).

The relationship between the measured curvature κ and the average stress $\overline{\sigma}$ is described by Stoney's equation:

$$\kappa = \frac{6}{M_s h_z^2} \overline{o} h_f \tag{1}$$

where h_s is the substrate thickness and M_s is the biaxial modulus of the substrate. h_f is the average film thickness, assuming that the film is relatively uniform and the surface roughness is not too large. $\bar{\sigma}$ is obtained by averaging the stress over the thickness of the film:

$$\overline{\sigma} = \frac{1}{h_f} \int_0^{h_f} \sigma_{xx}(z) dz \tag{2}$$

where $\sigma_{xx}(z)$ is the depth-dependent in-plane component of the stress, assumed to be equi-biaxial. $\overline{\sigma}h_f$ is often referred to as the stress-thickness or force per width.

During film growth, the stress-thickness may change due to the addition of new stressed layers at the surface, or by changing the stress in the layers that have already been deposited. The stress in newly-deposited layers $(\sigma_{xx}(h_f))$ is referred to as the incremental stress. If there is no change in the stress in existing layers, then the incremental stress is equal to the slope of the stress-thickness $(\frac{d(\bar{\sigma}h_f)}{dh_t})$.

2. Description of kinetic model

The kinetic model simulates the stress-thickness evolution through a rate equation that describes the rate of change of $\overline{o}h_f$ with thickness, i.e., $\frac{d(\overline{o}h_f)}{dh_f}$. The equation is based on several proposed mechanisms for the generation of stress during film growth [1,14]. The mechanisms are assumed to be additive, so that the effect of one is not affected by the other [15].

$$\frac{d(\overline{\sigma}h_f)}{dh_f} = \frac{d(\overline{\sigma}h_f)_{growth}}{dh_f} + \frac{d(\overline{\sigma}h_f)_{gg}}{dh_f} + \frac{d(\overline{\sigma}h_f)_{energetic}}{dh_f}$$
(3)

The terms on the right-hand-side of Eq. (3) correspond to the effects of growth kinetics, sub-surface grain growth, and energetic particle impingement. The analytical form for each of these terms is given below, along with a brief description of their physical origin and the meaning of the parameters. Further details can be found in the papers referenced in each section.

2.1. Growth kinetics

The stress-generating term referred to as 'growth kinetics' [14] describes mechanisms that have been proposed for non-energetic growth (e.g., evaporation or electrodeposition), represented schematically in Fig. 1. They focus on processes occurring at the top of the grain boundary between adjacent islands as the film grows, referred to as the

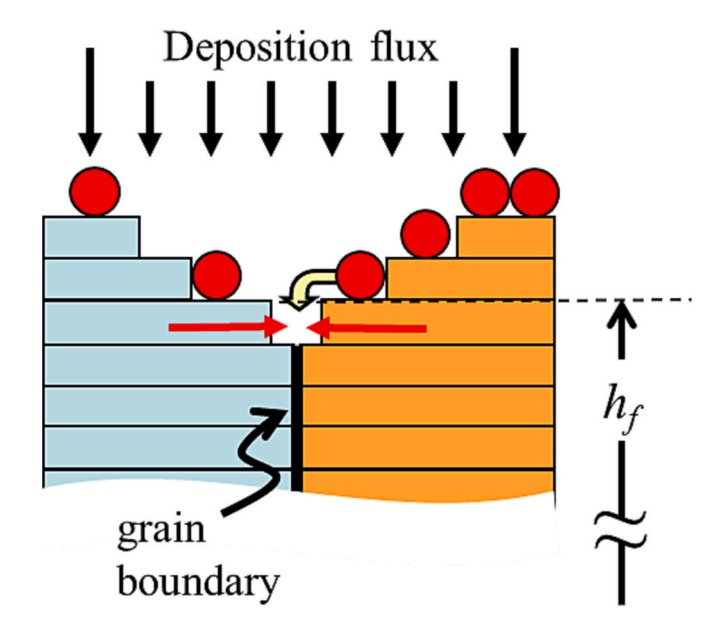


Fig. 1. Schematic of stress generating processes due to growth kinetics described in text. Red arrows represent tensile stress generated by formation of new segments of grain boundary. Yellow arrow represents compressive stress due to adatom diffusion into the grain boundary.

triple junction. This region is chosen because the crystalline symmetry is broken there, so that the region can be elastically deformed either by pulling the two neighboring grains closer together (tensile stress) or pushing them apart (compressive stress). One stress generation mechanism was proposed by Hoffman [16] in which tensile stress (represented by red arrows) is generated in each layer when the grain boundary initially forms. Because a grain boundary has fewer broken bonds than the surface of uncoalesced islands, it forms even at the expense of strain energy. The magnitude of the tensile stress (σ_T) is proportional to ($M_f \Delta \gamma/L_{surf}$) where M_f is the film's biaxial modulus, $\Delta \gamma$ is the difference between the surface and the grain boundary energy and L_{surf} is the grain size at the top of the triple junction.

A second mechanism proposes that compressive stress is generated by the diffusion of mobile atoms on the surface into the top of the triple junction (represented by the yellow arrow). The driving force for this process is attributed to the elevation of the chemical potential of atoms on the surface ($\delta\mu_s$) due to the flux of arriving atoms at the growth rate R. The consequent surface supersaturation increases the incorporation of atoms into the grain boundary which generates compressive stress in the film. In the model being discussed, the atoms are assumed to stay in the top of the triple junction, although other models assuming diffusion deeper into the grain boundary have also been developed [17].

The dynamic balance between these tensile and compressive stress generation mechanism leads to an incremental stress described by

$$\frac{d(\overline{\sigma}h_f)_{growth}}{dh_f} = \sigma_c + \left(\sigma_{T,0} \left(\frac{L_{ref}}{L_{surf}}\right)^{1/2} - \sigma_c\right) e^{\overline{\sigma_{surf}^{D}}}$$
(4)

where σ_c is the amount of compressive stress induced by the surface supersaturation and defined as $\sigma_C \equiv \delta \mu_S/\Omega$ where Ω is the atomic volume. β is a material-dependent kinetic constant and D is an effective diffusivity for hopping from the surface into the top of the grain boundary. Note that the term for σ_T has been separated into the products of two terms where $\sigma_{T,0}$ depends only on the material parameters while

the grain size dependence is expressed in the term $\left(\frac{L_{ref}}{L_{surf}}\right)^{1/2}$. L_{ref} is an arbitrary reference grain size so that $\sigma_{T,0}$ has units of stress. It is chosen to have a value of 1 nm for all the results described in this work.

The growth stress depends on the quantity RL/D, becoming more

tensile for higher values and more compressive for lower values. This explains several features of the experiments described in the background section: type I (tensile) behavior is seen for large growth rates and/or low temperatures while type II (compressive) behavior is seen for low growth rates or high temperatures. Increasing the grain size at the surface makes the stress less tensile for type I growth and less compressive for type II growth [18].

2.2. Effect of grain growth on stress

The grain size may change with the film thickness during deposition, both at the surface and throughout the thickness of the film. In Eq. (4) above for growth kinetics, the parameter L_{sturf} refers to the grain size at the surface. This term therefore already contains the dependence of $\frac{d(\bar{o}h_f)_{growth}}{dh_c}$ on grain size as the film grows.

However, this does not consider the effect of subsurface grain growth in the body of the film. As originally described by Chaudhari [11], this leads to additional stress because the grain boundary has a lower density than the rest of the film. As the grains grow, the number of grain boundaries decreases and therefore the dimensions of the film should decrease in the plane of the film. Since the film is attached to the substrate it cannot decrease its length and consequently develops a biaxial strain and corresponding stress. This assumes that the film remains dense and does not develop voids or other forms of porosity, which is not considered by this model.

Since the grain size may change with thickness, the depth-dependent grain size is defined as $L(z,h_f)$ where z is the height in the film relative to the substrate and h_f is the film thickness. The corresponding grain size at the surface is given by $L(h_f,h_f)$. Increasing the grain size at height z results in a strain in that layer of Δa $(1/L(z,z)-1/L(z,h_f))$ where Δa is the width of the grain boundary. The stress-thickness is determined by integrating the depth-dependent strain over the thickness of the film and multiplying by the biaxial modulus.

To make it possible to compute this stress, we assume that the average grain size changes linearly with the thickness:

$$L(z, h_f) = L_0 + \alpha_1 h_f + (\alpha_2 - \alpha_1)z$$

$$\tag{5}$$

where the parameters α_1 and α_2 describe the increase of the grain size at the film/substrate interface (z = 0) and film surface (z = h_f), respectively (the depth-dependent grain size is shown schematically in Fig. 2). This assumption is consistent with experimental studies [19]. The different modes of growth described by structure zone models [20,21] can be modelled by the appropriate choice of the grain growth parameters. For zone I (no grain growth), $\alpha_1 = \alpha_2 = 0$. For zone T (grain growth at surface only), $\alpha_1 = 0$. and $\alpha_2 > 0$. For zone II, (surface and subsurface grain growth), $\alpha_2 \ge \alpha_1 > 0$.

The effect of subsurface grain growth on the stress-thickness is given by [14]:

$$\frac{d\left(\overline{o}h_{f}\right)_{gg}}{dh_{f}} = M_{f} \Delta a \frac{\alpha_{1}h_{f}}{\left(L_{o} + \alpha_{1}h_{f}\right)\left(L_{o} + \alpha_{2}h_{f}\right)}$$

$$\tag{6}$$

Note that this term is zero if there is no grain growth at the film/substrate interface, i.e., α_1 =0. This term is positive so that increasing the grain size in the bulk of the film leads to an increase in the slope of the stress-thickness, corresponding to more tensile stress in the film.

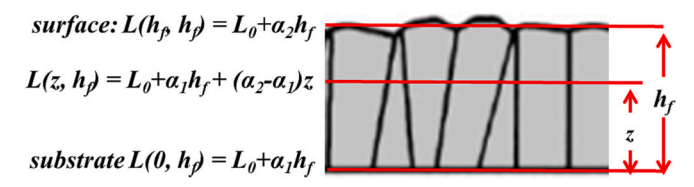


Fig. 2. Relationship between grain size at different depths and the parameters.

2.3. Effect of energetic particles

Additional processes must be considered for energetic deposition, as described more fully in ref. [22]. These are shown schematically in Fig. 3 for a single grain of size L. Energetic particles are assumed to impinge on the surface with flux f and implantation depth l. The surface moves upward at the growth rate R. There are two stress-generating mechanisms included in the model, depending on whether the energetic particle is incident near the grain-boundary or in the remaining bulk of the grain. The first mechanism is based on collision-induced densification of the atomic structure [23]. The shaded area in the figure (proportional to the implantation depth, *l*) represents the region in which the energetic species enhance incorporation of atoms into the grain boundary. We consider this to be a diffusion-less process by which atomic collisions within this region knock the atoms into more energetically favorable sites where compressive stress is generated. The stress from this mechanism is approximated by $A_o(\frac{l}{l})$ where A_o is a fitting parameter dependent on particle energy. This mechanism is designed to be consistent with studies by Magnfält et al. [24] that found an inverse grain size dependence of the compressive stress. It is also supported by molecular dynamics studies of particle-induced defects [25].

The second mechanism is associated with the introduction of mobile defects in the bulk of the film (i.e., not at the grain boundaries), sometimes referred to as subplantation in the literature [26,27]. As shown in Fig. 3, we assume that these defects (red circle) are created at a depth l from the surface that depends on the energy of the incoming particle. The resulting defect has a diffusivity D_l . The steady-state concentration (C_{ss}) of particle-induced defects depends on the incident defect flux ($c_o f$) as

$$C_{ss} = \frac{c_a f}{R} \frac{1}{\left(1 + \frac{l}{R \tau_s}\right)} \tag{7}$$

where τ_s is the characteristic time for the defect to diffuse to the surface that is moving upwards at a rate R. τ_s can be determined by equating the diffusion length with the distance to the surface:

$$\sqrt{D_i \tau_s} = l + R \tau_s \tag{8}$$

Defects that do not escape to the surface are assumed to remain trapped in the layer. The defect-induced stress is scaled by $(1-\frac{l}{L})$ because it is due to the fraction of energetic particles that are not within a distance l of the grain boundary.

The overall effect of these two mechanisms on the stress-thickness is given by

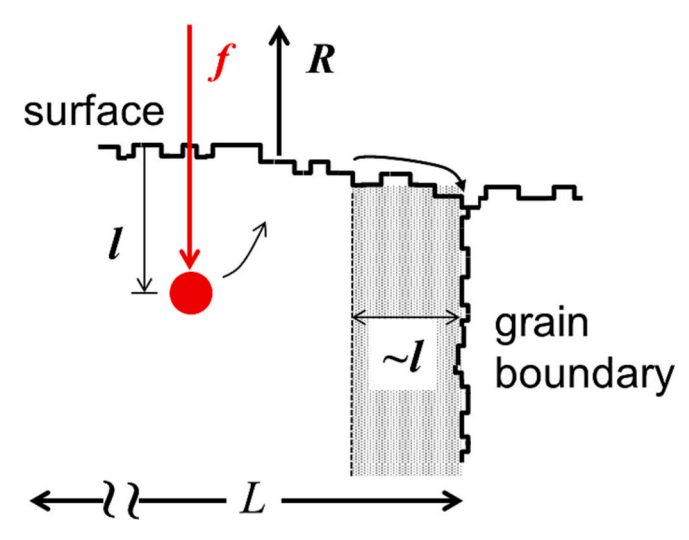


Fig. 3. Schematic of stress-generating processes in model for energetic growth.

$$\frac{d(\overline{o}h_f)_{energetic}}{dh_f} = A_o(l/L) + \left(1 - \frac{l}{L}\right) \frac{B_o}{\left(1 + \frac{l}{R\tau_s}\right)}$$
(9)

where B_0 is a parameter that includes the amount of stress per defect. The energetic parameters (A_0 and B_0) are expected to create more compressive stress at higher particle energy (lower pressure chamber) or larger ion/solid interaction. The A_0 term, due to densification at the grain boundary, is independent of the growth rate. The B_0 term, due to trapping of particle-induced defects, becomes more compressive at higher growth rates. It may saturate for high growth rates if all the defects are trapped in the growing layer.

3. Analysis using KMORFS computer program: results and discussion

The name of the program to analyze the film stress is KMORFS which is an acronym for Kinetic Model of Residual Film Stress. The program determines the kinetic parameters in the model by non-linear least squares fitting to minimize the difference between the data and the calculated values. Instructions for how to obtain the program and documentation describing its use are provided in Section 5. The documentation describes in detail the format of the two required files, one that contains the data and the other that contains the parameters and the constrains for the fitting.

An image of the graphical user interface is shown in Fig. 4. The 'Import' button is used to choose a parameter file that describes the initial guesses for all the fitting parameters and the constrains on the fitting. After the parameter file is entered, clicking the 'Calculate' button starts the fitting procedure. The format of the data files and parameter files is described in a user manual that is distributed with the program.

The program can be used to analyze curvature data in two modes, i. e., data for the slope of the stress-thickness (i.e., steady-state stress) or measurements of the curvature vs. thickness (stress-thickness evolution). These modes are described below.

3.1. Steady-state mode

If the slope of the curvature vs thickness measurements does not change with film thickness, then the stress is assumed to reach a steady-state. Two examples are discussed below, one for the case of stress in electrodeposited Ni at different growth rates and the other for stress in sputtered ZrN at different growth rates and pressures. Although σ_c may in principle depend on the growth conditions, it is assumed to have a single value for fitting the steady-state stress.

3.1.1. Electrodeposited Ni

An example is shown in Fig. 5 for electrodeposited Ni [8] where the steady-state stress is determined from the slope of the stress-thickness for several different growth rates (shown by red lines on Fig. 5a). The resulting steady-state stress vs. growth rate is shown by the symbols in Fig. 5b. The grain size was estimated to be the same for all the growth rates in the steady-state regime with a value of 100 nm.

Because this data is for non-energetic deposition and there is assumed to be no grain growth, the data can be fit using only the terms in the KMORFS model for growth kinetics (Eq. (4)). The model predicts that the stress depends on the growth rate through the term $e^{\frac{\rho D}{RL}}$. At small values of $\frac{\rho D}{RL}$, the stress approaches the compressive value of σ_c , while at large values it approaches $\sigma_{T,0}$. The result of fitting is shown by the solid line in Fig. 5b; the parameters are $\sigma_{T,0}=4.38$ GPa, $\sigma_c=-0.61$ GPa and $\beta D=104.2$ nm²/s.

For steady-state data in which the grain size is not all the same, the program allows a grain size to be entered for each data point. Studies of electrodeposited Cu [10] quantified the stress vs growth rate at different surface grain sizes (shown in Fig. 6). The grain size for each interval of growth at different rates was determined by using scanning electron microscopy on a cross-section of the sample made after the growth was finished. These data of stress vs. growth rate and grain size were also fit with the model using only 3 parameters. The result of fitting is shown by the surface in the figure; the fitting parameters are $\sigma_{T,0} = 1.93$ GPa, $\sigma_c = -0.016$ GPa and $\beta D = 1760$ nm²/s.

| KMORFS | + |
|--------|---|
| | KMORFS - Kinetic Model of Residual Film Stress Produced by Chason Research group, Brown University |
| | File Type *.xlsx ▼ |
| | Import ics.xlsx Calculate |
| | Steady State Stress Stress Thickness |
| | |
| | |
| | |
| | |
| This v | right © 2023. rork is licensed under a <u>Creative Commons Attribution-NoDerivatives 4.0 International License,</u> details regarding how the generic license terms apply specifically to KMORFS can be found <u>here.</u> |

 $\textbf{Fig. 4.} \ \ \text{KMORFS user interface.}$

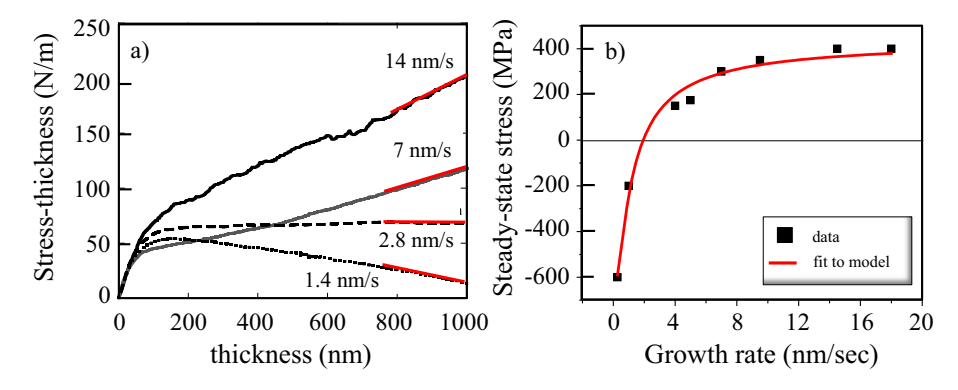


Fig. 5. a) The slope of the stress-thickness (red lines) is used to obtain the steady-state stress at different deposition rates. b) The steady-state stress vs. growth rate. The red line is calculated from a fit to the model.

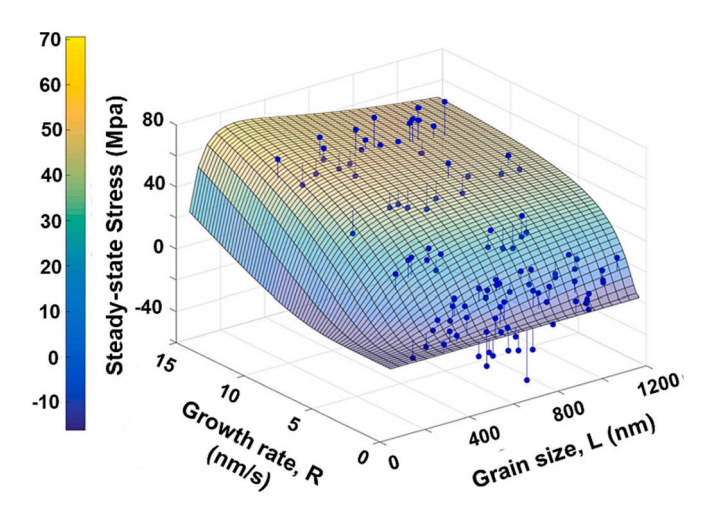


Fig. 6. Measurements (circles) and fit (surface) for measurements of Cu steady-state stress at different growth rates and grain sizes.

3.1.2. Sputter-deposited ZrN

Measurements of steady-state stress in sputtered ZrN made at different pressures and growth rates are shown as the symbols in Fig. 7 [28]. To reduce the number of free parameters, the model assumes that the energetic parameters have a linear dependence on pressure so that

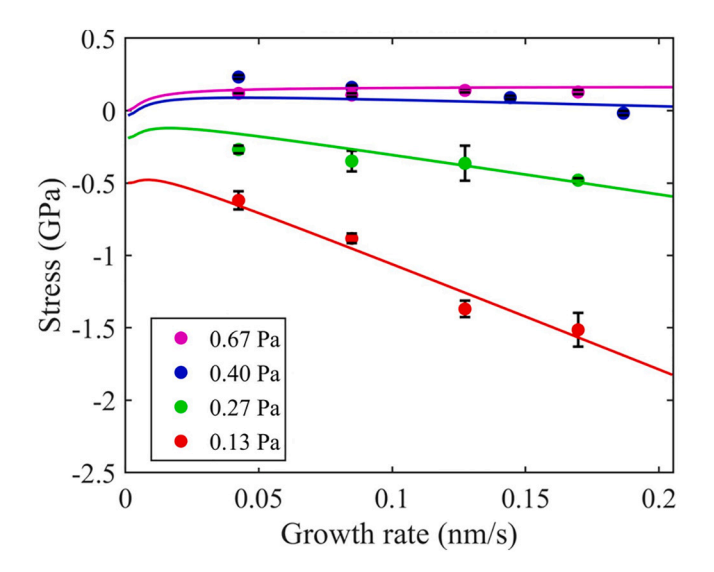


Fig. 7. Steady-state stress in sputter-deposited ZrN vs. growth rate at different pressures indicated in figure. The solid lines are fits to the model.

 $A_o(P)=A^{'*}\left(1-\frac{P}{P_o}\right)$ where A' and P₀ are the fitting parameters. Similar pressure dependence was used for $B_o(P)$ and l(P). The other parameters $(\sigma_{T,0},\sigma_c,\beta D,D_i)$ were made to have the same fitting value for all of the sets of data.

The results for fitting the stress measured at different R and P are shown in Fig. 7. The corresponding fitting parameters are shown in Table 1. The fitting results on the figure (solid line) indicate that the model is able to explain the growth rate and pressure dependence of the stress observed in the measurements. For each growth rate, the stress becomes more compressive when the pressure is lowered. This is attributed to the fact that the stress from energetic particle impingement is larger for low pressure. It also affects the growth rate dependence of the stress so that at lower pressure the stress becomes more compressive as the growth rate is increased than it does at higher pressure (lower particle energy).

3.2. Stress-thickness mode

The model can also be used to analyze the evolution of the stress-thickness with thickness. This is necessary for systems where the grain size changes during growth so that the slope of the stress-thickness does not reach a steady-state value. Additional parameters $(M_f\Delta a, \alpha_1, \alpha_2, L_0)$ are included in the fitting to account for the grain growth. The model can fit data for evaporated films, sputter-deposited films or both evaporated and sputtered data simultaneously for the same material. Because the mechanisms in the model assume that the film is relatively uniform in thickness, it should only be applied to the stress-thickness data in the range of thicknesses after coalescence has occurred (i.e., after the tensile peak in the early stages of growth). The program allows the starting value of thickness for the fitting to be specified.

3.2.1. Evaporated Ni

Measurements of stress-thickness vs. thickness for evaporated Ni are shown in Fig. 8. These data are from Yu and Thompson [29] who measured the stress at different temperatures at a growth rate of 0.05 nm/s and at different growth rates for a temperature of 373 K. The processing conditions for each data set are indicated by the color, and can be found in Table 2. The slope of the stress-thickness changes continuously with thickness, which indicates that the grain size is not constant.

The parameters obtained from fitting the model are shown in Table 2. One of the strengths of the program is that it can analyze multiple sets of data simultaneously, and parameters can be made to be common to all the data sets (material-dependent) or allowed to vary for each set of data (process-dependent). Since there is separate data for each set of growth conditions, we allow σ_c to have different values for the fitting of each stress-thickness file (process-dependent). However, the program also allows the fitting to be done with a common value of σ_c

Table 1Fitting parameters for sputtered ZrN corresponding to results in Fig. 7. The solid lines are fits to the model.

| | $\sigma_c \\ (\text{GPa})$ | $\sigma_{T,0}$ (GPa) | βD (nm^2/s) | $D_i \\ (nm^2/s)$ | P ₀ (Pa) | A* (GPa) | B* (GPa) | l* (nm) |
|-----|----------------------------|----------------------|----------------------|-------------------|------------------------|-------------|-------------|------------|
| ZrN | -0.01 | 0.13 | 0.30 | 6.20 | 0.48 | -142.11 | -274.41 | 0.31 |

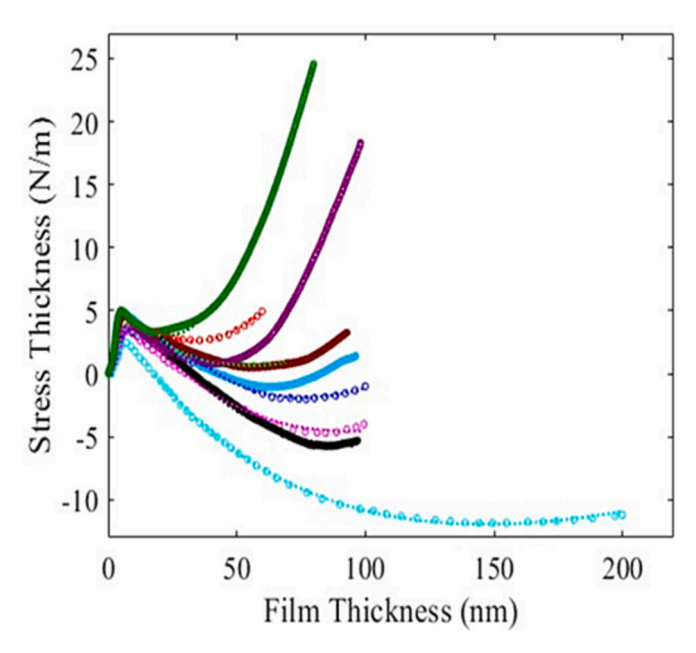


Fig. 8. Stress-thickness vs. thickness in evaporated Ni at different temperatures and growth rates. The processing conditions corresponding to each color are shown in Table 2. The solid lines are fits to the model.

Table 2Fitting parameters for evaporated Ni corresponding to results in Fig. 8. The upper panel contains fitting parameters that are common to all the data sets (material-dependent). The lower panel contains fitting parameters that are allowed to vary for each data set (process-dependent).

| Fitting Parameters Common to All Files | | | | | | | | |
|--|----------------------------------|---------------------|------------------|--|--|--|--|--|
| $\sigma_{T,0}$ (GPa) | $ \beta D (T = 300K) (nm2/s) $ | E _A (eV) | Mf∆a (GPa*nm) | | | | | |
| 4.56 | 2.06 | 0.16 | 35.6 | | | | | |

| R (nm/s) | T (K) | σ _c (GPa) | $egin{array}{c} L_o \ (m{nm}) \end{array}$ | α1 | α2 |
|----------|----------|-------------------------|--|------|------|
| 0.05 | 300 | -4.29 | 10.31 | 0.02 | 0.03 |
| 0.05 | 333 | -3.72 | 20.72 | 0.02 | 0.07 |
| 0.05 | 398 | -2.90 | 30.34 | 0.10 | 0.23 |
| 0.05 | 423 | -2.95 | 49.30 | 0.12 | 0.33 |
| 0.05 | 473 | -2.11 | 47.69 | 0.00 | 0.48 |
| 0.03 | 373 | -3.59 | 55.05 | 0.33 | 0.50 |
| 0.05 | 373 | -2.78 | 22.51 | 0.07 | 0.07 |
| 0.08 | 373 | -3.74 | 17.93 | 0.04 | 0.04 |
| 0.13 | 373 | -5.86 | 6.96 | 0.05 | 0.05 |
| 0.25 | 373 | -6.01 | 5.57 | 0.01 | 0.01 |

for all the files (material-dependent). The upper panel contains the material-dependent fitting parameters and the lower panel contains process-dependent fitting parameters.

3.2.2. Sputter-deposited Ni

The model can also fit the stress-thickness evolution for sputtered

films. Similar to the steady-state stress examples above, additional terms for the energetic parameters are included in the fitting relative to the fitting of evaporated films. The energetic parameters are assumed to depend linearly on the pressure below a threshold value in order to reduce the number of fitting parameters.

Results for sputter-deposited Ni are shown for 3 pressures (0.27, 0.67 and 1.33 Pa) at a growth rate of 0.076 nm/s and a temperature of 293 K. The fitting parameters are in Table 3 and the stress-thickness data is compared with the model fit in Fig. 9. Note how the stress becomes more compressive at lower pressures for the same growth rate and temperature. Further details of the fitting can be found in [30].

4. Discussion

The examples presented in the sections above show how the KMORFS computational model can be used to analyze either the steady-state stress or the stress-thickness evolution in a number of systems. Further results for evaporated film systems (Ag, Cu, Ni, Fe, Ti, Cr) [14] and sputter-deposited films (Cu, Ni, Co, Cr, Mo, W) [1] can be found in the associated manuscripts for other data that have been presented in the literature.

It is instructional to compare the results of evaporation and sputter-deposition of the same material, e.g., Ni [1]. The results show that the same parameters for non-energetic growth can be used to explain both the evaporated and sputter-deposited data. This supports the assumption of the model that the different stress-generating processes can be considered as additive [15]. In other words, the parameters controlling stress in non-energetic deposition are still appropriate for explaining the non-energetic component of the stress in energetic deposition.

The validity of the model can also be explored by comparing the results of the fitting with physical parameters obtained by other methods. For instance, measurements of the grain size (where available) are compared with the results predicted by the fitting at the same film thickness in ref. [14] for evaporated thin films. Although the agreement is not perfect, the model results are similar to the measurements which show that the fitting parameters are reasonable. The activation energy for the βD fitting parameter is also shown to be proportional to the melting point of the different materials studied. This is consistent with the observation that the activation energy for diffusion is proportional to

Table 3Fitting parameters for sputtered Ni corresponding to results in Fig. 9. The upper panel contains fitting parameters that are common to all the data sets (material-dependent). The lower panel contains fitting parameters that are allowed to vary for each data set (process-dependent).

| Fitting Parameters Common to All Files | | | | | | | | |
|--|---|-------|------|------|------------|------------|------|--|
| $\beta D \\ (300K) \\ (nm^2/s)$ | $\begin{pmatrix} \zeta \\ \zeta \end{pmatrix} \begin{pmatrix} \sigma_{T,0} \\ (\text{GPa}) \end{pmatrix} \begin{pmatrix} Mf\Delta a \\ (\text{GPa*nm}) \end{pmatrix}$ | | Di | (Pa) | A * | B * | l* | |
| 4.46 | 7.18 | 33.65 | 6.50 | 0.65 | -1.31 | -1.0 | 1.71 | |

| R (nm/s) | T (K) | P (Pa) | σ _c (GPa) | $L_o (nm)$ | α1 | α2 |
|----------|----------|-----------|-------------------------|------------|------|------|
| 0.076 | 293 | 0.27 | -0.82 | 18.68 | 0.16 | 0.20 |
| 0.076 | 293 | 0.670 | -1.09 | 4.02 | 0.21 | 0.36 |
| 0.076 | 293 | 1.33 | -0.97 | 3.47 | 0.30 | 0.50 |

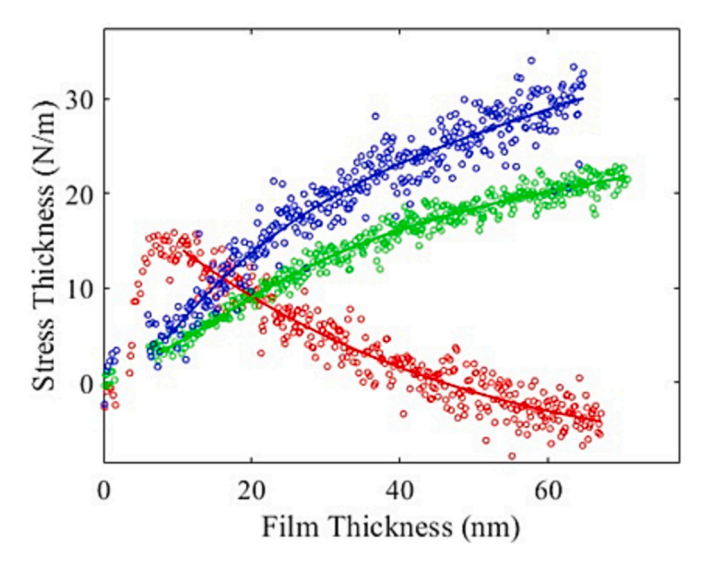


Fig. 9. Stress-thickness vs. thickness in sputtered Ni at different pressures. The processing conditions corresponding to each color are shown in Table 3. The solid lines are fits to the model.

the melting point for many transition metals. Similarly, the activation energy for the defect diffusion fitting parameter (D_i) is shown to scale with the melting point in ref. [1].

Assuming that the model adequately represents the mechanisms that control film stress, the question remains as to what is the utility of being able to model film stress and determine the kinetic parameters. At the most basic level, analyzing curvature data allows the film grower to determine what are the most important processes that control the stress. Each mechanism has a different signature dependence on the growth rate, pressure and microstructural evolution. For instance, if the stress becomes more tensile at higher growth rates, it is likely dominated by growth kinetics. But if the stress becomes more compressive at higher growth rates, then the effects of energetic particle bombardment are likely to be more important. Knowing what the dominant stressinducing mechanism is can determine which parameters can be tuned most efficiently to obtain a desired stress state.

To be more quantitative, the values of the kinetic parameters obtained from the data fitting can be used to predict how the stress will evolve under different growth conditions. For example, consider the evolution of stress with thickness, such as the data for evaporated Ni discussed in Section 3.2.1. The change in stress-thickness with thickness $(\frac{d(\bar{o}h_f)}{dh_f})$ can be calculated from Eqs. (4) and (6) using the fitting parameters. This type of information can be used to produce schemes for film growth in which the growth temperature is adjusted as a function of thickness to produce a film with zero curvature (using appropriate corrections for the thermal-expansion induced stress). Such a complex set of growth conditions (i.e., a thickness-dependent deposition temperature) would be difficult to determine without the insight provided by the stress model.

As the KMORFS program is used to analyze stress measurements from many different materials systems (from our own research and that of others), a database of kinetic parameters will be developed and shared on a website. This will provide guidance to users on what conditions should be used for growing films to obtain desired levels of stress. In this way, a user can benefit from the prior work of others to shorten the number of experiments that need to be done to optimize the growth conditions.

5. Obtaining the KMORFS program for use by thin film growers

The KMORFS program is available free of charge to any researchers

who are interested in using it to analyze thin film stress measurements. It can be obtained by sending a request to Eric_Chason@Brown.edu. The user will be sent a link to download a package containing the KMORFS software, associated documentation describing how to use it and a set of data and parameter files for several examples (similar to those described above). For users who have access to the MATLAB® software, they can download an app that can be run. For users who do not have access to MATLAB, a standalone version is also available.

6. Conclusion

A computational tool (KMORFS) for analyzing the evolution of residual thin film stress has been developed with a user-friendly interface to make it accessible to the community of thin film growers. Based on the fundamental kinetic processes that contribute to stress, the KMORFS program produces a set of kinetic parameters for the analyzed material that can be used to predict the stress under different processing conditions. The model has been used to analyze data for many types of materials systems (metals and metal-nitride) and multiple deposition methods (evaporation, electrodeposition, and sputter-deposition).

The program is available for no cost to researchers to analyze their own stress measurements. The results of work by different groups will be collected into a database that can help users choose the growth conditions that will give a desired stress state for a wide range of materials. The database will also reveal how the kinetic parameters depend on a material's physical properties so that the model can be further improved. In the future, this may allow the kinetic parameters for the model to be determined from first principles calculations instead of fitting the data. This would enable a film grower to determine the best conditions for producing a film with desired stress without having to do a large number of experiments to determine the parameters.

Currently, work is being done to extend the stress model to consider alloy films in addition to the elemental films that have been studied previously. If this work is successful, it will allow the estimation of stress in films with a combination of elements using the kinetic parameters determined from studies of the constituent elemental films.

CRediT authorship contribution statement

Eric Chason: Conceptualization, Methodology, Resources, Writing – original draft, Writing – review & editing, Visualization, Supervision, Project administration, Funding acquisition.

Tong Su: Software development, Validation, Formal analysis, Investigation, Data curation, Writing – original draft, Writing – review & editing, Visualization.

Zhaoxia Rao Software development, data analysis, Writing – review and editing.

Declaration of competing interest

(Chason, ICMCTF)

The authors declare that they have no known competing financial interests or personal relationships that could have appeared to influence the work reported in this paper.

Data availability

Data will be made available on request.

Acknowledgements

The effort of TS and EC was supported by the National Science Foundation (NSF) under Contract DMR-2006422. We thank Prof. Diederik Depla (Ghent U.) and Prof. Greg Thompson (U. of Alabama) for useful input.

References

- [1] T. Su, Z.X. Rao, S. Berman, D. Depla, E. Chason, Analysis of stress in sputter-deposited films using a kinetic model for Cu, Ni, Co, Cr, Mo, W, Appl. Surf. Sci. 613 (2023) 156000, https://doi.org/10.1016/j.apsusc.2022.156000.
- [2] M.F. Doerner, W.D. Nix, Stresses and deformation processes in thin-films on substrates, CRC Crit. Rev. Solid State Mater. Sci. 14 (1988) 225–268, https://doi. org/10.1080/10408438808243734.
- [3] R. Koch, The intrinsic stress of polycrystalline and epitaxial thin metal-films,
 J. Physics-Condens. Matter 6 (1994) 9519–9550, https://doi.org/10.1088/0953-8984/6/45/005.
- [4] R. Koch, Stress in evaporated and sputtered thin films a comparison, Surf. Coat. Technol. 204 (2010) 1973–1982, https://doi.org/10.1016/j.surfcoat.2009.09.047.
- [5] E. Chason, P.R. Guduru, Tutorial: understanding residual stress in polycrystalline thin films through real-time measurements and physical models, J. Appl. Phys. 119 (2016) 191101, https://doi.org/10.1063/1.4949263.
- [6] G. Abadias, E. Chason, J. Keckes, M. Sebastiani, G.B. Thompson, E. Barthel, G. L. Doll, C.E. Murray, C.H. Stoessel, L. Martinu, Review article: stress in thin films and coatings: current status, challenges, and prospects, J. Vac. Sci. Technol. A 36 (2018) 020801 https://doi.org/10.1116/J.5011790
- [7] R. Abermann, Measurments of the intrinsic stress in thin metal films, Vacuum 41 (1990) 1279–1282, https://doi.org/10.1016/0042-207x(90)93933-a.
- [8] S.J. Hearne, J.A. Floro, Mechanisms inducing compressive stress during electrodeposition of Ni, J. Appl. Phys. 97 (2005), 014901, https://doi.org/ 10.1063/1.1819972
- [9] S.C. Seel, C.V. Thompson, S.J. Hearne, J.A. Floro, Tensile stress evolution during deposition of Volmer–Weber thin films, J. Appl. Phys. 88 (2000) 7079–7088, https://doi.org/10.1063/1.1325379.
- [10] A.M. Engwall, Z. Rao, E. Chason, Residual stress in electrodeposited Cu thin films: understanding the combined effects of growth rate and grain size, J. Electrochem. Soc. 164 (2017) D828–D834, https://doi.org/10.1149/2.0921713jes.
- [11] P. Chaudhari, Grain-groath and stress relief in thin-films, J. Vac. Sci. Technol. 9 (1972) 520-522. https://doi.org/10.1116/1.1316674.
- [12] J.A. Thornton, D.W. Hoffman, Stress-related effects in thin films, Thin Solid Films 171 (1989) 5–31, https://doi.org/10.1016/0040-6090(89)90030-8.
- [13] L.B. Freund, S. Suresh, Thin Film Materials, Cambridge University Press, 2003.
- [14] Z.X. Rao, S. Berman, P.L. Yang, D. Depla, E. Chason, Understanding residual stress in thin films: analyzing wafer curvature measurements for Ag, Cu, Ni, Fe, Ti, and Cr with a kinetic model, J. Appl. Phys. 130 (2021) 135304, https://doi.org/10.1063/ 5.0058919
- [15] G.C.A.M. Janssen, J.D. Kamminga, Stress in hard metal films, Appl. Phys. Lett. 85 (2004) 3086–3088, https://doi.org/10.1063/1.1807016.
- [16] R. Hoffman, Stresses in thin films relevance of grain boundaries and impurities, Thin Solid Films 34 (1976) 185–190, https://doi.org/10.1016/0040-6090(76) 90453-3

- [17] E. Chason, A.M. Engwall, Z. Rao, T. Nishimura, Kinetic model for thin film stress including the effect of grain growth, J. Appl. Phys. 123 (2018) 185305, https://doi. org/10.1063/1.5030740.
- [18] A.M. Engwall, Z. Rao, E. Chason, Origins of residual stress in thin films: interaction between microstructure and growth kinetics, Mater. Des. 110 (2016) 616–623, https://doi.org/10.1016/j.matdes.2016.07.089.
- [19] A. Dulmaa, F.G. Cougnon, R. Dedoncker, D. Depla, On the grain size-thickness correlation for thin films, Acta Mater. 212 (2021) 116896, https://doi.org/ 10.1016/j.actamat.2021.116896.
- [20] J.A. Thornton, The microstructure of sputter-deposited coatings, J. Vac. Sci. Technol. A 4 (1986) 3059–3065, https://doi.org/10.1116/1.573628.
- [21] I. Petrov, P.B. Barna, L. Hultman, J.E. Greene, Microstructural evolution during film growth, J. Vac. Sci. Technol. A 21 (2003) S117–S128, https://doi.org/ 10.1116/1.1601610.
- [22] E. Chason, M. Karlson, J.J. Colin, D. Magnfalt, K. Sarakinos, G. Abadias, A kinetic model for stress generation in thin films grown from energetic vapor fluxes, J. Appl. Phys. 119 (2016) 145307, https://doi.org/10.1063/1.4946039.
- [23] K.-H. Müller, Ion-beam-induced epitaxial vapor-phase growth: a molecular-dynamics study, Phys. Rev. B 35 (1987) 7906–7913, https://doi.org/10.1103/PhysRevB 35 7906
- [24] D. Magnfält, G. Abadias, K. Sarakinos, Atom insertion into grain boundaries and stress generation in physically vapor deposited films, Appl. Phys. Lett. 103 (2013), 051910. https://doi.org/10.1063/1.4817669.
- [25] M. Zhang, Z.X. Rao, K.S. Kim, Y. Qi, L. Fang, K. Sun, E. Chason, Molecular dynamics simulation of stress induced by energetic particle bombardment in Mo thin films, Materialia 16 (2021) 101043, https://doi.org/10.1016/j. mtla.2021.101043.
- [26] P. Patsalas, C. Gravalidis, S. Logothetidis, Surface kinetics and subplantation phenomena affecting the texture, morphology, stress, and growth evolution of titanium nitride films, J. Appl. Phys. 96 (2004) 6234–6246, https://doi.org/ 10.1063/1.1811389.
- [27] Y. Lifshitz, S. Kasi, J. Rabalais, Subplantation model for film growth from hyperthermal species - application to diamond, Phys. Rev. Lett. 62 (1989) 1290–1293, https://doi.org/10.1103/PhysRevLett.62.1290.
- [28] Z.X. Rao, E. Chason, Measurements and modeling of residual stress in sputtered TiN and ZrN: dependence on growth rate and pressure, Surf. Coat. Technol. 404 (2020) 126462, https://doi.org/10.1016/j.surfcoat.2020.126462.
- [29] H.Z. Yu, C.V. Thompson, Grain growth and complex stress evolution during Volmer–Weber growth of polycrystalline thin films, Acta Mater. 67 (2014) 189–198, https://doi.org/10.1016/j.actamat.2013.12.031.
- [30] T.R. Koenig, Z.X. Rao, E. Chason, G.J. Tucker, G.B. Thompson, The microstructural and stress evolution in sputter deposited Ni thin films, Surf. Coat. Technol. 412 (2021) 126973, https://doi.org/10.1016/j.surfcoat.2021.126973.